# Modeling, Analysis and Simulation of a Hybrid Multifunctional System Applied to Wind Generation

**Joham Lucas Dos Santos Albuquerque** [*] **Isaac Rocha Machado** [**]
**Samelius Silva De Oliveira** [**] **Alan Robson De Sousa Silva** [*]

[*] *Faculdade de Engenharia Elétrica, Universidade Federal do Ceará, CE(e-mail: joham_lucas@hotmail.com, alanrsilva@alu.ufc.br).*
[**] *PPGEEC/UFC, Universidade Federal do Ceará, CE (e-mail: isaacmachado@ufc.br, samelius1@gmail.com).*

**Abstract:** This work proposes a hybrid wind power generation system connected to the power grid through a back-to-back converter. The Grid Side Converter (GSC), connected to the eletric grid via an L filter, mitigates harmonic currents and corrects the power factor of a non-linear load connected to the Point of Common Coupling (PCC). The Machine Side Converter (MSC) implements the Rotor Field Oriented Control (RFOC) in dq Synchronous Reference Frames (SRF). This technique enables independent and decoupled control of the torque and magnetization of the Squirel Cage Induction Generator (SCIG). The torque reference is obtained through the Maximum Power Point Tracking - Optimal Torque (MPPT-OT), this method tracks the maximum power point based on the calculation of the optimal electromagnetic torque obtained from the measurement of the mechanical speed of the generator.

*Keywords:* Wind power generation, integrated active filter, harmonic filtering, power quality, maximum power point traking, squirrel-cage induction generator.

## 1. INTRODUCTION

Currently, it is increasingly common to use multifunctional power generation systems in the literature. The need to use electronic power converters in Distributed Generation (DG) systems and the need to add features related to the power quality motivated the development of the work. In addition, other benefits such as cost optimization, reduction of the installation volume and the gain of added value (economic and technological) to existing technologies are the main advantages of the proposed topology and a control system.

The studies presented in Martins (2018) and Ferreira (2005) detail a rotor flux oriented control of a Squirrel Cage Induction Generator (SCIG) coupled to a wind turbine. The SCIG is connected to the Point of Common Coupling (PCC) via a Back-to-Back converter. In Ferreira (2005) the system is developed based on the instantaneous powers theory. In Martins (2018), on the other hand, there is a focus on the power quality comparing the operation of the wind generation system coupled to the power grid through an L filter and an LCL filter. In Mishra and Saha (2018) a SCIG supplies a non-linear load forming an islanded system. With no active filtering and no connection to the power grid, the control of the load side converter is based on maintaining the AC voltage, while the DC bus voltage control is carried out by the generator side converter. In Moreira et al. (2019), control strategies for a wind power system with a Double Feed Induction Generator (DFIG) were proposed. The machine's rotor is connected to the power grid via a back-to-back converter that has an additional active filter function implemented from the grid side converter.

In Chen and Wang (2016) it is presented an application of a Unified Power Quality Conditioner (UPQC) in the transient compensation of a wind generation system. Current harmonics caused by power grid imbalances and voltage distortions are mitigated, with the SCIG connected directly to the power grid. The UPQC is connected to the PCC and consists of a back-to-back converter with one side converter operating as a parallel active filter and the other side converter as a dynamic voltage restorer.

In Kumar and Chatterjee (2016) and Huang et al. (2015) bibliographic reviews are made and the state of the art of classic and iterative methods for MPPT algorithms applied to wind generation is presented. The works present similar techniques but with small differences in the application method, however the works do not include systems with mechanical coupling from a gearbox.

This work proposes the control of a wind system as well as its optimization through a maximum power extraction strategy. It also aims to improve the quality of energy injected into the electrical grid through an active filtering system implemented in the grid-side converter.

## 2. PROPOSED SYSTEM

The system proposed in this work is shown in Fig. 1, which is a hybrid system that adds as a feature of active parallel filtering and wind generation from the control of a SCIG.

The distributed generation system consists of a Squirrel-Cage Induction Generator that is connected via a back-to-back converter coupled to the network using an L filter. The maximum power tracking method used is the Maximum Power Point Tracking Optimal Torque (MPPT-OT) which it consists of calculating the optimal torque for maximum power extraction by measuring the mechanical speed of the generator rotor and based on known parameters of the wind turbine.

The vector control of the currents of the converter on the generator side is based on the rotor flux, and is also known as the FOC method. Method widely used in modern literature because, in reference dq, a natural decoupling between magnetization fluxes and electromagnetic torque (Oliveira, 2016). Being an indirect approach, because the rotor flux is not measured, but estimated.

Regarding the Grid Side Converter (GSC), the control of active and reactive power is done through the vectorial control of currents, which has two control loops used to regulate currents in direct axis and in quadrature, respectively. For this, the angle of the synchronism circuit must be aligned with the spatial voltage vector of the PCC, which is equivalent to having the angular argument equal to that of the phase A voltage of the PCC. The synchronism circuit used is the Synchronous Reference Frame Phase-Locked Loop (PLL-SRF), a Phase-Locked Loop (PLL) configuration based on the Park transform that obtains the reference angle of the dq plane from the cancellation of the voltage in the quadrature axis.

Harmonic mitigation of adjacent loads is done by incorporating harmonic components to the current references of the GSC controller by obtaining the current in the load in synchronous reference. And the correction of the load power factor is done through the current control in the quadrature axis of the GSC.

## 3. WIND TURBINE

The mechanical power developed in the wind turbine shaft is given by (1) (Boyle, 1996; Martins, 2018; Kumar and Chatterjee, 2016).

$$P_{tur} = \frac{1}{2} C_p(\lambda, \beta).\rho_a.A_a.v_v^3 \tag{1}$$

Where: $\rho_a$: Volumetric air density ($kg/m^3$), $A_a$: Wind turbine area ($m^2$), $v_v$: Wind speed ($m/s$).

The wind turbine power coefficient ($C_p$) is a function of the tip velocity ratio ($\lambda$) and the pitch angle ($\beta$) and is given by (Kumar and Chatterjee, 2016):

$$C_p(\lambda, \beta) = k_1 \left( \frac{k_2}{\lambda_i} - k_3\beta - k_4\beta^{k_5} - k_6 \right) e^{\left(-\frac{k_7}{\lambda_i}\right)} \tag{2}$$

$$\frac{1}{\lambda_i} = \frac{1}{\lambda + 0.08\beta} - \frac{0.035}{1 + \beta^3} \tag{3}$$

Where: $k_1$, $k_2$, $k_3$, $k_4$ e $k_5$: Constructive parameters of the wind turbine. The $ks$ coefficients used in this work are (Kumar and Chatterjee, 2016): $k_1 = 0.73$, $k_2 = 151$, $k_3 = 0.58$, $k_4 = 0.002$, $k_5 = 2.14$, $k_6 = 13.2$ e $k_7 = 18.4$.

The tip speed ratio is given by (4) (Boyle, 1996; Martins, 2018; Kumar and Chatterjee, 2016).

$$\lambda = \frac{\omega'_m.R_{tur}}{v_w} \tag{4}$$

Where: $\omega'_m$: Mechanical angular speed of the turbine ($rad/s$), $R_{tur}$: Wind turbine radius ($m$).

The analysis of the wind potential in the analyzed scenario is based on the Weibull distribution, which is a probability density function given by (Riaz and Khan, 2019):

$$f_{wb}(v_v) = \frac{k}{c} \left( \frac{v_v}{c} \right)^{k-1} e^{\left(-\frac{v_v}{c}\right)^k} \tag{5}$$

Where: $f_{wb}$: Weibull probability density function. c: Scale factor, k: Weibull shape factor.

In Ayodele et al. (2012) it is defined for which optimal wind speed a wind turbine should be designed given the Weibull distribution ($v_{v,opt}$), given by:

$$v_{v,opt} = c \left( 1 + \frac{2}{k} \right)^{\frac{1}{k}} \tag{6}$$

Knowing that the turbine area is given by $\pi R_{tur}^2$, substituting in (7) and considering that the maximum power extracted by the turbine in $v_v = v_{v,opt}$ equals the nominal power of the generator ($P_0$), a wind turbine sizing equation is reached:

$$R_{tur} = \sqrt{\frac{2P_0}{\pi C_{p,max} \rho_a v_{v,opt}^3}} \tag{7}$$

Where: $C_{p,max}$: maximum wind turbine power coefficient.

The statistical distribution of winds in the analyzed scenario has a scale factor (c) of 6.6 m/s and a shape factor (k) of 3.2. For these values $v_{v,opt} = 7.68\ m/s$.

Based on the model of the wind turbine used in this work, and defining that the wind turbine will have a fixed pitch angle at 0°, the following values are obtained: $C_{p,max} = 0.4412$. The value of $\lambda$ that results in the value of $C_{p,max}$ ($\lambda_{opt}$) is 5.66.

Knowing further that the average air density for that scenario is 1.09 $kg/m^3$ and that the nominal power of the generator used is $15kW$, the projected radius of the turbine will be approximately $6.62m$.

## 4. GEARBOX

The mechanical model of the generator given by (8) and (9) and the mechanical transformation equations given by (10) and (11) (Leonhard, 2001).

$$J\frac{d\omega_m}{dt} + B\omega_m = T_e - T_c \tag{8}$$

$$T'_c = \frac{P_{tur}}{\omega'_m} \tag{9}$$

$$\omega_m = N.\omega'_m \tag{10}$$

$$T_c = \frac{1}{N} T'_c \tag{11}$$

Where: $J$: Total moment of inertia referenced to the generator side, $B$: Viscous friction coefficient referenced to the generator side. $\omega_m$: Mechanical angular speed of the turbine on generator shaft. $T_e$: Electromagnetic torque on generator, $T_c$: Mechanical torque on generator shaft, $T'_c$:

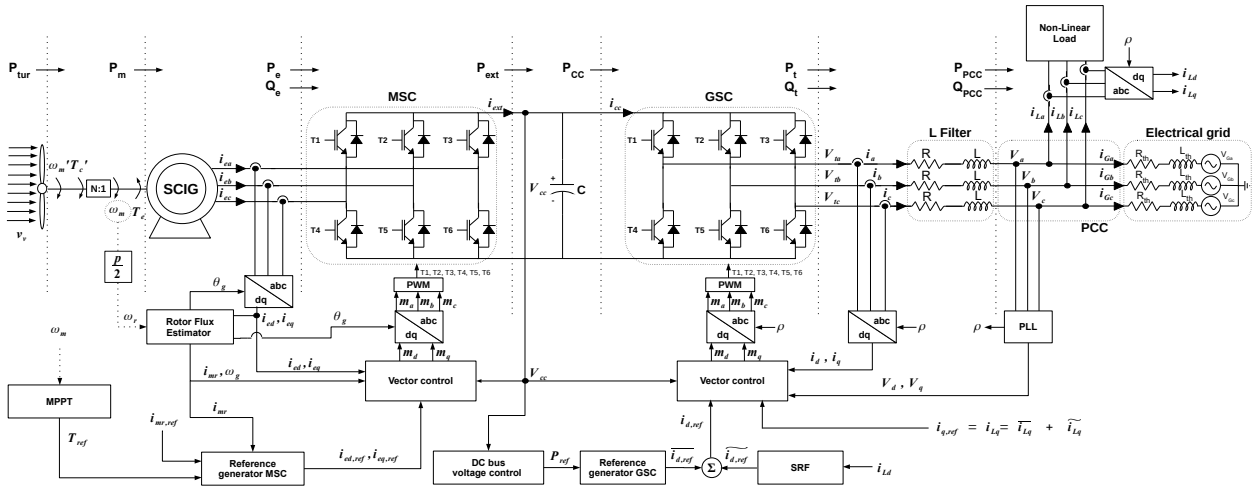


Figure 1. Schematic diagram of the proposed system.

Mechanical torque on turbine shaft, $N$: Gearbox mechanical transformation ratio.

The wind turbine nominal angular speed value ($\omega'_{m,nom}$) is obtained by substituting the optimum operating values of the wind turbine in (4), as (12).

$$\omega'_{m,nom} = \frac{\lambda_{opt} v_{v,opt}}{R_{tur}} \tag{12}$$

The nominal angular speed of the generator is given by (Chapman, 2013):

$$\omega_{m,nom} = \frac{2\pi f_0}{p/2} \tag{13}$$

Where: $f_0$: Nominal stator frequency ($Hz$), $p$: Number of generator poles. Which are 60 $Hz$ and 4 poles, respectively.

In order to make the nominal values of turbine and generator rotation compatible, (12) and (13) are replaced in (10):

$$N = \frac{\omega_{m,nom}}{\omega'_{m,nom}} = \frac{2\pi f_0 R_{tur}}{(p/2)\lambda_{opt} v_{v,opt}} \tag{14}$$

Results in: $N \approx 28.7$.

## 5. MACHINE SIDE CONVERTER

The SCIG equations in space vector notation are given by (Leonhard, 2001; Yazdani and Iravani, 2010):

$$\overrightarrow{v_r} = R_r \overrightarrow{i_r} + L_r \frac{d\overrightarrow{i_r}}{dt} + L_m \frac{d(\overrightarrow{i_e} e^{-j\theta_r})}{dt} \tag{15}$$

$$\overrightarrow{v_e} = R_s \overrightarrow{i_e} + L_s \frac{d\overrightarrow{i_e}}{dt} + L_m \frac{d(\overrightarrow{i_r} e^{j\theta_r})}{dt} \tag{16}$$

$$\sigma_r = \frac{L_r}{L_m} - 1, \qquad L_r = (1+\sigma_r) L_m \tag{17}$$

$$\sigma_s = \frac{L_s}{L_m} - 1, \qquad L_s = (1+\sigma_s) L_m \tag{18}$$

$$\sigma = 1 - \frac{L_m^2}{L_s L_r} = 1 - \frac{1}{(1+\sigma_s)(1+\sigma_r)} \tag{19}$$

$$\tau_r = \frac{L_r}{R_r} = \frac{L_m(1+\sigma_r)}{R_r} \tag{20}$$

$$\tau_s = \frac{L_s}{R_s} = \frac{L_m(1+\sigma_s)}{R_s} \tag{21}$$

Where: $v_r$: Rotor voltage, $v_e$: Stator voltage, $i_r$: Rotor current, $i_e$: Stator current, $R_r$: Rotor electrical resistance, $R_s$: Rotor electrical resistance, $R_s$: stator, $L_r$: Self-inductance of the rotor, $L_s$: Self-inductance of the stator, $L_m$: Mutual inductance between stator and rotor, $\sigma_r$: Scattering factor of the rotor, $\sigma_s$: Scattering factor of stator, $\sigma$: Total dispersion factor, $\tau_r$: Rotor time constant, $\tau_s$: Stator time constant, $\theta_r$: Electrical angular position of the rotor.

### *5.1 Rotor flux estimator*

The equations (22) and (23) define the rotor flux ($\Psi_r$) and the rotor magnetizing current ($i_{mr}$) (Leonhard, 2001; Yazdani and Iravani, 2010).

$$\overrightarrow{\Psi}_r = \Psi_r e^{j\theta_r} = L_m \overrightarrow{i_{mr}} = L_m[(1+\sigma_r)\overrightarrow{i_r} e^{j\theta_r} + \overrightarrow{i_e}] \tag{22}$$

$$\overrightarrow{i_{mr}} = i_{mr} e^{j\theta_g} \tag{23}$$

Where: $\theta_g$: Angular position of the rotor flux.

Developing (15) based on (17), (20), (22) and (23) and considering that due to the squirrel cage rotor configuration, $\overrightarrow{v_r} = 0$, results in (24), (25) and (26) (Yazdani and Iravani, 2010). Which are the rotor flux estimator model, represented in Fig. 2.

$$i_{mr} = \frac{i_{ed}}{\tau_r s + 1} \tag{24}$$

$$\omega_g = \omega_r + \frac{i_{eq}}{\tau_r i_{mr}} \tag{25}$$

$$\theta_g = \int_0^t \omega_g dt \tag{26}$$

### *5.2 SCIG vector control in rotor field coordinates*

Developing (16) based on (18), (19) and (21) results in (27), (28), (29) and (30) (Yazdani and Iravani, 2010).

$$u_{1d} = i_{ed} + \sigma\tau_s \frac{di_{ed}}{dt}; \tag{27}$$

$$u_{1q} = i_{eq} + \sigma\tau_s \frac{di_{eq}}{dt}; \tag{28}$$

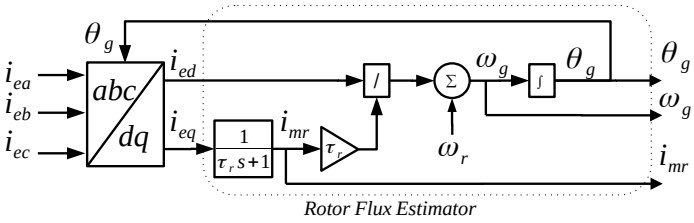


Figure 2. Rotor flux estimator.

$$\frac{v_{ed}}{R_s} = u_{1d} + \tau_s(1-\sigma)\frac{di_{mr}}{dt} - \omega_g\tau_s\sigma i_{eq} \quad (29)$$

$$\frac{v_{eq}}{R_s} = u_{1q} + \omega_g\tau_s(1-\sigma)i_{mr} + \omega_g\tau_s\sigma i_{ed} \quad (30)$$

Where: $u_{1d}$ and $u_{1q}$: Linearized control inputs for the MSC direct axis and quadrature axis current controllers, respectively.

The transfer function of the current loop oriented to the rotor flux is given by:

$$G_m(s) = \frac{i_{ed}(s)}{u_{1d}(s)} = \frac{i_{eq}(s)}{u_{1q}(s)} = \frac{1}{\sigma\tau_s s + 1} \quad (31)$$

Based on (27), (28), (29), (30) and (30) and (31), the block diagram of the SCIG current controller is shown in Fig. 3.

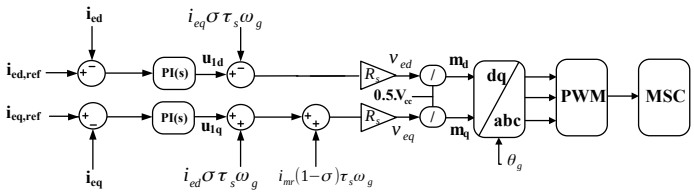


Figure 3. Vector control of currents of the MSC.

## 6. REFERENCES TO MSC DRIVERS

### *6.1 Direct axis current reference*

The direct axis stator current reference ($i_{ed,ref}$) is obtained from the magnetizing current reference ($i_{mr,ref}$), and is given by (32) (Yazdani and Iravani, 2010).

$$i_{ed,ref} = i_{mr,ref} = \sqrt{\frac{2}{3}}\frac{V_{e-ll0}}{(1+\sigma_s)L_m 2\pi f_0} \quad (32)$$

Where: $V_{e-ll0}$: SCIG nominal line voltage.

Calculating (32), gives $i_{ed,ref} = i_{mr,ref} = 12.72\ A$.

### *6.2 Quadrature axis current reference*

The SCIG electromagnetic torque ($T_e$) is given in terms of the magnetizing current and the quadrature axis current according to (33) (Ferreira, 2005).

$$T_e = \frac{3}{2}\frac{p}{2}\left(\frac{L_m}{1+\sigma_r}\right)i_{mr}i_{eq} = \frac{3}{2}\frac{p}{2}(1+\sigma_r)L_s i_{mr}i_{eq} \quad (33)$$

Based on (33), the quadrature axis stator current reference ($i_{eq,ref}$) can be expressed from the reference torque ($T_{ref}$ ) according to (34).

$$i_{eq,ref} = T_{ref}\frac{4}{3p}\left(\frac{1+\sigma_r}{L_m}\right)\frac{1}{i_{mr}} \quad (34)$$

### *6.3 Obtaining the reference torque through the MPPT-OT*

The MPPT-OT is the calculation of the optimal reference torque given the operating point with the best efficiency of the turbine, that is, $Cp, max$.

The turbine simulated in this work operates with a fixed pitch angle at 0°, which implies that, theoretically, the optimum operating point always occurs for the same tip speed ratio value ($\lambda_{opt}$) .

Replacing (4) in (1), and replacing the turbine area by $\pi R_{tur}^2$, the power generated by the wind turbine with the aforementioned mechanical quantities next to the turbine is:

$$P_{tur} = \frac{1}{2}\rho_a\pi R_{tur}^5\frac{C_p(\lambda,\beta)}{\lambda^3}\omega_m'^3. \quad (35)$$

By replacing (35) in (9), the mechanical torque referred to the wind turbine will be:

$$T_c' = \frac{1}{2}\rho_a\pi R_{tur}^5\frac{C_p(\lambda,\beta)}{\lambda^3}\omega_m'^2. \quad (36)$$

Substituting the optimal operating values, the reference torque for operating at the maximum power extraction point referred to the mechanical axis of the wind turbine is (Kumar and Chatterjee, 2016):

$$T_{ref}' = \frac{1}{2}\rho_a\pi R_{tur}^5\frac{C_{p,max}}{\lambda_{opt}^3}\omega_m'^2. \quad (37)$$

Applying the transformations proposed in (10) and (11), the reference torque referred to the mechanical axis of the generator is given by (38).

$$T_{ref} = \frac{1}{2N^3}\rho_a\pi R_{tur}^5\frac{C_{p,max}}{\lambda_{opt}^3}\omega_m^2. \quad (38)$$

## 7. GRID SIDE CONVERTER

Equation (39) is the GSC voltage equation in space vector notation (Moreira et al., 2019; Yazdani and Iravani, 2010; Martins, 2018).

$$\overrightarrow{V_t} = R\overrightarrow{i} + L\frac{d\overrightarrow{i}}{dt} + \overrightarrow{V} \quad (39)$$

Where: $V_t$: Voltage at the terminals of the GSC, $V$: Voltage at the PCC, $i$: Line current of the GSC, $R$: L Filter resistance, $L$: L Filter inductance.

### *7.1 GSC vector control in synchronous reference*

By developing (39) it is possible to arrive at the following equations (Moreira et al., 2019; Yazdani and Iravani, 2010; Martins, 2018):

$$u_{2d} = Ri_d + L\frac{di_d}{dt} \quad (40)$$

$$u_{2q} = Ri_q + L\frac{di_q}{dt} \quad (41)$$

$$V_{td} = u_{2d} - L\omega_s i_q + V_d \quad (42)$$

$$V_{tq} = u_{2q} + L\omega_s i_d + V_q \quad (43)$$

Where: $\omega_s$: Angular frequency of the electrical grid, $u_{2d}$ and $u_{2q}$: Linearized control inputs for the GSC direct axis and quadrature axis current controllers, respectively.

### 7.2 PLL

The transfer function of PLL is given in (44) (Moreira et al., 2019).

$$G_{PLL}(s) = \frac{v_q(s)}{\omega(s)} = \frac{V}{s} \tag{44}$$

As a consequence of the configuration used: $V_q = 0$.

### 7.3 DC bus

The transfer function representing the dynamic of the DC bus voltage ($G_v$) is given in (45) and (45) (Yazdani and Iravani, 2010; Moreira et al., 2019).

$$G_v(s) = \frac{V_{cc}^2(s)}{P_{PCC}(s)} = -\left(\frac{2}{C}\right)\frac{\tau s + 1}{s} \tag{45}$$

$$\tau = \frac{2LP_{PCC0}}{3V_d^2} \tag{46}$$

Where: $V_{cc}$: DC bus voltage, $P_{PCC}$: Active power sent to the electrical grid, $C$: DC bus capacitance, $P_{PCC0}$: Value of $P_{PCC}$ where the transfer function has been linearized around it.

### 7.4 SRF Algorithm

Because of the PLL configuration, in steady state $V_q = 0$, with this the equations of active power ($P_{PCC}$) and reactive power ($Q_{PCC}$) in the common coupling point can be written according to (47) and (48) (Moreira et al., 2019; Yazdani and Iravani, 2010).

$$P_{PCC} = \frac{3}{2}\left[V_d i_d\right] \tag{47}$$

$$Q_{PCC} = \frac{3}{2}\left[-V_d i_q\right] \tag{48}$$

Decomposing the GSC line currents into their continuous ("—") and oscillating ("~") components:

$$i_d = \overline{i_d} + \widetilde{i_d} \tag{49}$$

$$i_q = \overline{i_q} + \widetilde{i_q} \tag{50}$$

The current control references of the GSC are obtained according to the diagram in Fig. 4 where $\widetilde{i_{d,ref}}$ and $\widetilde{i_{q,ref}}$ are responsible for harmonic mitigation and $\overline{i_{q,ref}}$ for power factor correction at fundamental frequency, and are obtained from the load current ($i_L$) (Moreira et al., 2019).

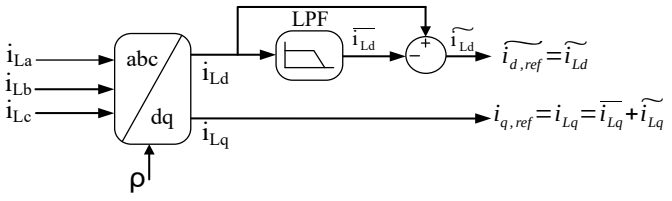


Figure 4. Current references generated by the load.

The Low Pass Filter (LPF) used in the SRF algorithm is a second order filter with a cutoff frequency of $12Hz$. The $\overline{i_{d,ref}}$ reference is taken from the DC bus voltage controller. Thus, the complete MSC control system is shown in Fig. 5.

## 8. CONTROLLERS PROJECT

The controllers used in this work are PI controllers whose transfer function is given by (51) (KATHUSHIKO, 2011):

$$PI(s) = k_p\left(1 + \frac{1}{T_i s}\right) \tag{51}$$

The parameters $k_p$ and $T_i$ of the controllers are taken from (52) and (53) (KATHUSHIKO, 2011; Moreira et al., 2019).

$$T_i = \frac{1}{\omega_c \,.\, tg\left(\pi + \angle OPTF(j\omega_c) - PM_d\right)} \tag{52}$$

$$k_p = \frac{1}{|OPTF(j\omega_c)|\,.\left|\left(1 - \frac{j}{T_i\omega_c}\right)\right|} \tag{53}$$

Where: $OPTF$: System open-loop transfer function, $\omega_c$: Gain crossover frequency, $T_i$: Integrative time, $PM_d$: Desired phase margin.

The block diagrams of the system controllers are shown in Fig. 6. The block $J_p(s)$ in Fig. 6b is a closed-loop transfer function of the GSC controller, expressed by (54).

$$J_p(s) = \frac{G_p(s).PI_p(s)}{1 + G_p(s).PI_p(s)} \tag{54}$$

In the design of the DC link voltage controller, for positive values of $P_{PAC0}$ and $\tau$ the converter is operating as an inverter, and it operates as a rectifier when these values are negative. Therefore, for the project of this controller, $\tau = 0$ can be considered as a particular case of the project (Moreira et al., 2019). For $\tau = 0$, the transfer function $G_v(s)$ is expressed as (55).

$$G_v(s) = -\left(\frac{2}{C}\right)\frac{1}{s} \tag{55}$$

System controller gains are obtained based on (52) and (53). Where $PM_d$ and $\omega_c$ are the basic project parameters. Thus, the values of $PM_d$ and $\omega_c$ chosen for each system controller and their respective gains obtained are shown in Table 1.

## 9. SIMULATION RESULTS

In the first simulation, a three-phase diode rectifier show in Fig. 7 was used as a non-linear load with the following parameters: Active power: $13.23kW$, Fundamental Reactive power: $0.64kVA$, Current THD 29.34%, Power Factor: 0.958. Simulated in the following intervals: Interval 1 (from 1 to 2.1 s) - Only active filtering function; Interval 2 (from 2.1 to 3 s) - Active filtering and wind energy management functions (with $v_v = 7.68m/s$); Interval 3 (from 3 to 4 s) - only wind energy management function (with $v_v = 7.68m/s$).

Fig. 8 shows the voltage reference ($V_{cc,ref}$) and the DC bus voltage ($V_{cc}$). In this image, the operating steps of the system are presented.

Fig. 9 shows (within interval 1, with the system working only as an active filter) the three-phase line currents in the non-linear load, in the GSC and in the power grid.

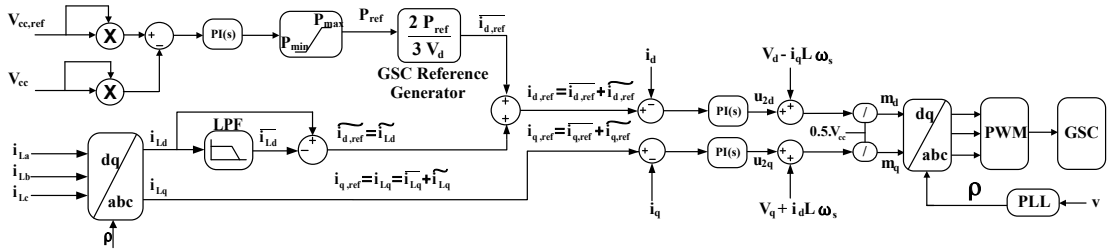


Figure 5. GSC control diagram.

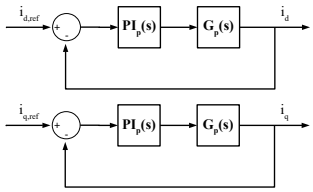

(a) Block diagram of GSC current controllers.

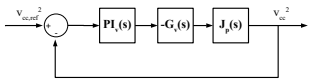

(b) Block diagram of the DC bus voltage controller.

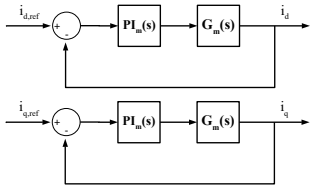

(c) Block diagram of MSC current controllers.

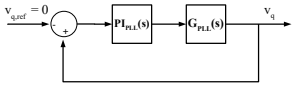

(d) Block diagram of the PLL controller.

Figure 6. System control loops.

Table 1: System controller gains.

| **GSC current controllers** | | | |
|---|---|---|---|
| ***Project values*** | | ***Parameters obtained*** | |
| $\omega_c$ | $4.52 \times 10^6\ rad/s$ | $k_p$ | 7690.62 |
| $PM_d$ | 89.9999° | $T_i$ | 0.1266 |
| **DC bus voltage controller** | | | |
| ***Project values*** | | ***Parameters obtained*** | |
| $\omega_c$ | $60\ rad/s$ | $k_p$ | 0.0405 |
| $PM_d$ | 40° | $T_i$ | 0.01396 |
| **MSC current controllers** | | | |
| ***Project values*** | | ***Parameters obtained*** | |
| $\omega_c$ | $4.52 \times 10^6\ rad/s$ | $k_p$ | 70794.84 |
| $PM_d$ | 89.9999° | $T_i$ | 0.0139 |
| **PLL controller** | | | |
| ***Project values*** | | ***Parameters obtained*** | |
| $\omega_c$ | $5654.86\ rad/s$ | $k_p$ | 18.1 |
| $PM_d$ | 85° | $T_i$ | 0.00202 |

The grid current on at intervals 1, 2 and 3 is shown in Fig. 10. The current THD obtained were 0.59%, 7.46% and 30.2% for intervals 1, 2 and 3 respectively.

The power factors at fundamental frequency were 1, 1 and 0.857 for intervals 1, 2 and 3, respectively. While the total power factor (considering the THD) were 0.99997, 0.997 and 0.269 for intervals 1, 2 and 3, respectively.

On the SCIG side, the magnetization of the machine depends directly on the rotor flux estimator and the current vector control. Fig.11a shows the direct axis reference current and the magnetizing current obtained in SCIG.

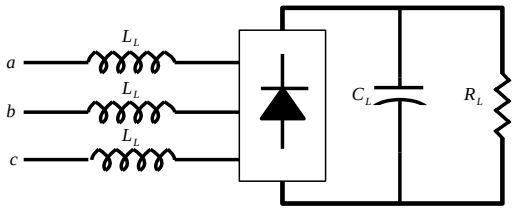


Figure 7. Non-linear load.

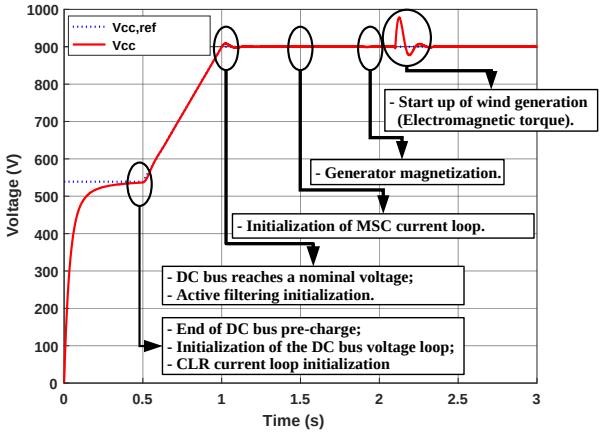


Figure 8. DC bus voltage.

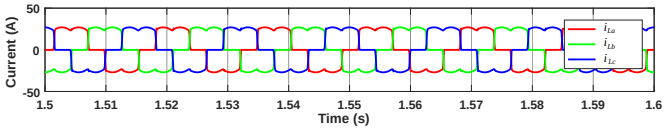


(a) Load currents during interval 1.

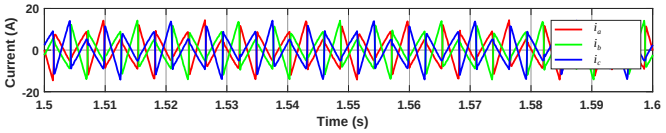


(b) GSC currents during interval 1.

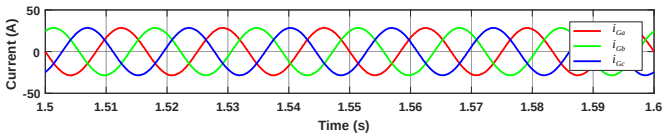


(c) Grid currents during interval 1.

Figure 9. Load, GSC and grid currents during interval 1.

Fig. 11b shows the current references and currents synthesized in the SCIG stator in *dq* reference frame.

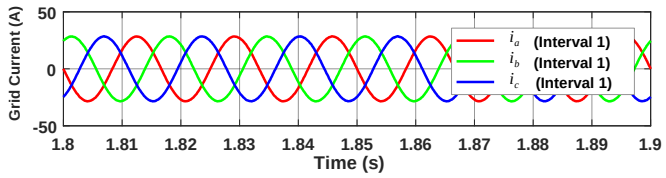


(a) Grid currents for intervals 1.

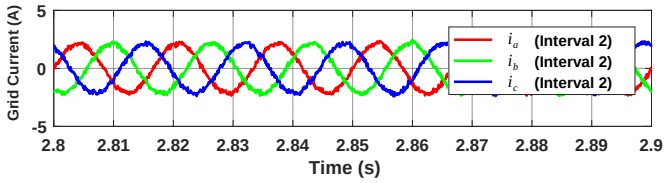


(b) Grid currents for intervals 2.

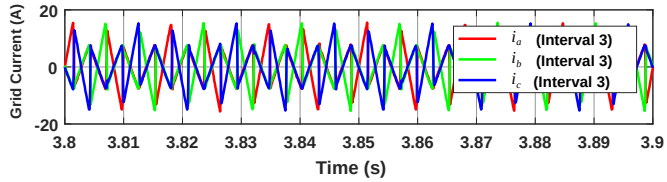


(c) Grid currents for intervals 3.

Figure 10. Grid currents for intervals 1, 2 and 3.

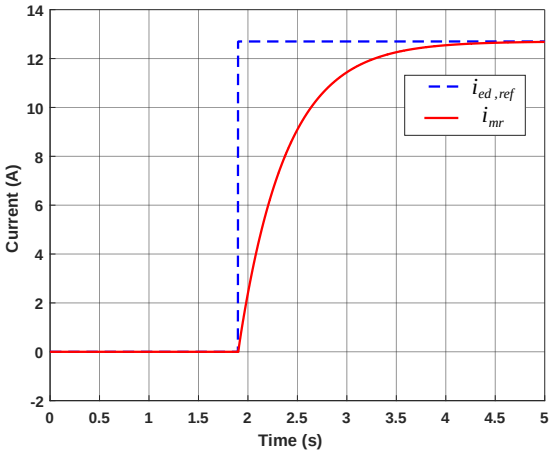


(a) Induction machine magnetizing current.

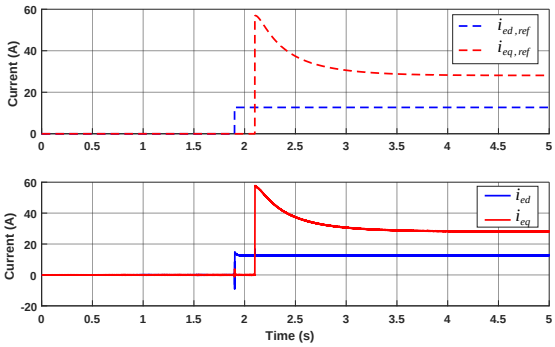


(b) Currents in dq reference frame in the induction machine.

Figure 11. Currents in SCIG.

In the second part of the simulation, the MPPT for variable wind speed show in Fig. 12a was analyzed.

The Fig. 12b presents the power curves in the MPPT analysis. Where $P_{max}$ is the theoretical maximum extractable power.

Faced with a variable wind speed profile, variations in the reference torque cause the quadrature-axis stator current reference to oscillate similarly to the reference torque, as shown in Fig. 12c.

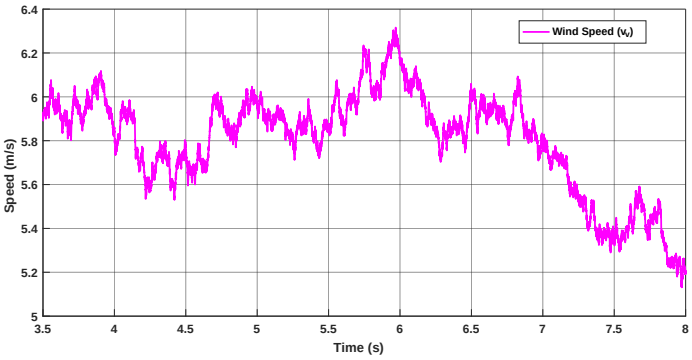


(a) Wind speed profile.

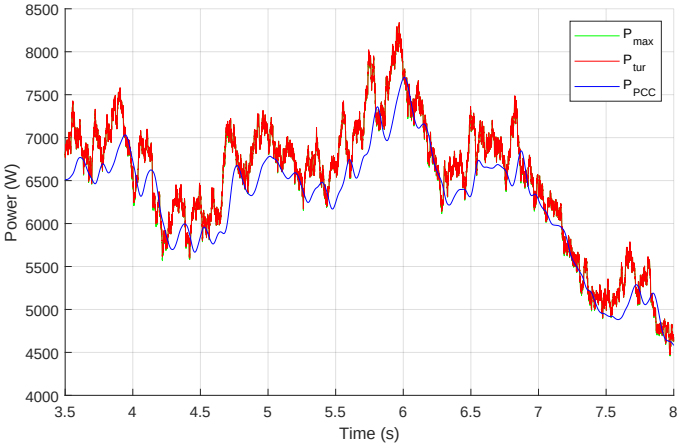


(b) Tracking the maximum power point.

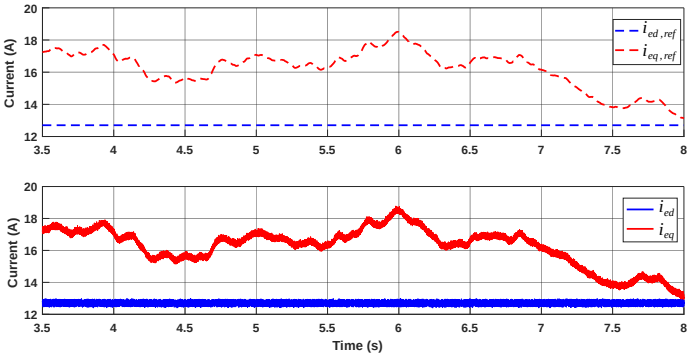


(c) Currents in dq reference frame in the induction machine for a variable wind profile.

Figure 12. MPPT results.

## 10. CONCLUSION

In the analysis of the system regarding active filtering, during interval 1, a THD 0.59% in the current can be observed, respecting the design parameters being, even, within the limit values in the IEEE 519:2014 standard, which is 5% at its lowest rate. And during the comparison

between intervals 2 and 3, a significant improvement in the quality of electric power can be observed when the system operates with active filtering and wind generation instead of when the system operates only with wind generation. In interval 2, a current THD of 7.46% was obtained. In interval 3, the observed current THD was 302%. Thus, the presence of the active filtering functionality decreased the current harmonic distortion by 97.53% when comparing intervals 2 and 3.

The power factor at fundamental frequency was unity for intervals 1 and 2. The total power factor was 0.99997 and 0.997 for intervals 1 and 2, respectively. While for interval 3, where there is no power factor correction, the fundamental frequency power factor and the total power factor were 0.857 and 0.269, respectively.

Analysis of the THD and power factor data shows that active filtering significantly improved the electrical power quality of the system.

In the MPPT analysis, the oscillating wind profile was obtained from the integration of a white noise generator around the average wind speed of the analyzed scenario. The graphs of maximum extractable power ($P_{max}$) from the wind and of power on the axis of the wind turbine are practically superimposed, which shows the effectiveness of the maximum power tracking method implemented and the guarantee of fast dynamics to the current controllers of the Machine Side Converter (MSC). However, the active power sent to the PCC ($P_{PCC}$) on almost the entire chart is less than the power on the wind turbine axis ($P_{tur}$), this is mainly due to losses in the induction machine and cannot be attributed to switching losses, as the semiconductor devices used in the simulation are practically ideal. At specific moments $P_{PCC}$ was greater than $P_{tur}$, which shows the inertia of the system due to the slow dynamics of the DC bus and the dynamics of other peripherals in the system.

The simulation results obtained good dynamic performances, validating the hybrid control technique proposed.

## REFERENCES

Ayodele, T.R., Jimoh, A.A., Munda, J.L., and Agee, J.T. (2012). Statistical analysis of wind speed and wind power potential of port elizabeth using weibull parameters. *Journal of Energy in Southern Africa*, 23(2), 30–38.

Boyle, G. (1996). *Renewable energy: power for a sustainable future*. Oxford University Press.

Chapman, S.J. (2013). *Fundamentos de máquinas elétricas*. AMGH Editora.

Chen, W.L. and Wang, M.J. (2016). Design of dynamic voltage restorer and active power filter for wind power systems subject to unbalanced and harmonic distorted grid. In *2016 IEEE Applied Power Electronics Conference and Exposition (APEC)*, 3471–3475. IEEE.

Ferreira, J.C.d.C. (2005). *Aplicação do controle vetorial e teoria PQ no controle de aerogeradores conectados à rede elétrica*. Master's thesis, Programa de Engenharia Elétrica, COPPE UFRJ.

Huang, C., Li, F., and Jin, Z. (2015). Maximum power point tracking strategy for large-scale wind generation systems considering wind turbine dynamics. *IEEE Transactions on Industrial Electronics*, 62(4), 2530–2539.

KATHUSHIKO, O. (2011). Engenharia de controle moderno. 5º edição. *Editora LTC*.

Kumar, D. and Chatterjee, K. (2016). A review of conventional and advanced mppt algorithms for wind energy systems. *Renewable and sustainable energy reviews*, 55, 957–970.

Leonhard, W. (2001). *Control of electrical drives*. Springer Science & Business Media.

Martins, G.S. (2018). *Técnicas de controle de potências ativa e reativa utilizando gerador de indução gaiola de esquilo aplicado a um sistema de geração eólica*. Master's thesis, Universidade Estadual de Campinas.

Mishra, R. and Saha, T.K. (2018). Control of scig based distributed power generation scheme supplying nonlinear and unbalanced load. In *2018 IEEE International Conference on Power Electronics, Drives and Energy Systems (PEDES)*, 1–6. IEEE.

Moreira, A.B., Barros, T.A.D.S., Teixeira, V.S.D.C., Souza, R.R.D., Paula, M.V.D., and Filho, E.R. (2019). Control of powers for wind power generation and grid current harmonics filtering from doubly fed induction generator: Comparison of two strategies. *IEEE Access*, 7, 32703–32713. doi:10.1109/ACCESS.2019.2899456.

Oliveira, C.M.R.d. (2016). *Controle vetorial da máquina de indução por modos deslizantes integral utilizando método de anti-windup*. Ph.D. thesis, Universidade de São Paulo.

Riaz, M.M. and Khan, B.H. (2019). Estimation of weibull parameters and selection of optimal wind turbine for the development of large offshore wind farm. In *2019 International Conference on Electrical, Electronics and Computer Engineering (UPCON)*, 1–6. IEEE.

Yazdani, A. and Iravani, R. (2010). *Voltage-sourced converters in power systems: modeling, control, and applications*. John Wiley & Sons.

## Appendix A. SIMULATION DATA

Wind turbine: $\beta$ = Fixed on 0°, $J = 50x10^{-3}\ Kg.m^2/rad$, $B = 587.9x10^{-9}\ Kg.m^2/rad.s$.

SCIG: $P_0 = 15\ kW$, $V_{e-ll0} = 460$ V, $f_0 = 60\ Hz$, p = 4 poles, $R_s = 276.1\ m\Omega$, $R_r = 164.5\ m\Omega$, $L_m = 76.14\ mH$, $L_s = 78.331\ mH$, $L_r = 78.331\ mH$.

Electrical grid: $V_{LL} = 381.05$ V, $f_s = 60\ Hz$, $R_{th} = 0\ \Omega$, $L_{th} = 0\ H$.

L Filter: $R = 0\ \Omega$, $L = 1.7\ mH$.

DC bus: $C = 2.1\ mF$, Control voltage = 900 V.

Non-linear load: $R_L = 20\ \Omega$, $L_L = 100\ \mu H$, $C_L = 2\ \mu F$.

MSC and GSC: Switching frequency = $30\ kHz$.